PKD-dependent PARP12-catalyzed mono-ADP-ribosylation of Golgin-97 is required for E-cadherin transport from Golgi to plasma membrane

Giovanna Grimaldi[a,b,1], Angela Filograna[a,b], Laura Schembri[b], Matteo Lo Monte[a,b], Rosaria Di Martino[a,b], Marinella Pirozzi[a,b], Daniela Spano[b], Andrea R. Beccari[c], Seetharaman Parashuraman[a,b], Alberto Luini[a,b,1], Carmen Valente[a,b,1], and Daniela Corda[d,1]

[a]Institute for Endocrinology and Experimental Oncology "G. Salvatore," National Research Council, 80131 Naples, Italy; [b]Institute of Biochemistry and Cell Biology, National Research Council, 80131 Naples, Italy; [c]Drug Discovery Platform, Dompé Farmaceutici SpA Research Center, 67100 L'Aquila, Italy; and [d]Department of Biomedical Sciences, National Research Council, 00185 Rome, Italy

Edited by Pascale Cossart, Unité des Interactions Bacteries-Cellules, Institut Pasteur, Paris, France; received December 24, 2020; accepted November 15, 2021

Adenosine diphosphate (ADP)-ribosylation is a posttranslational modification involved in key regulatory events catalyzed by ADP-ribosyltransferases (ARTs). Substrate identification and localization of the mono-ADP-ribosyltransferase PARP12 at the *trans*-Golgi network (TGN) hinted at the involvement of ARTs in intracellular traffic. We find that Golgin-97, a TGN protein required for the formation and transport of a specific class of basolateral cargoes (e.g., E-cadherin and vesicular stomatitis virus G protein [VSVG]), is a PARP12 substrate. PARP12 targets an acidic cluster in the Golgin-97 coiled-coil domain essential for function. Its mutation or PARP12 depletion, delays E-cadherin and VSVG export and leads to a defect in carrier fission, hence in transport, with consequent accumulation of cargoes in a *trans*-Golgi/Rab11–positive intermediate compartment. In contrast, PARP12 does not control the Golgin-245–dependent traffic of cargoes such as tumor necrosis factor alpha (TNFα). Thus, the transport of different basolateral proteins to the plasma membrane is differentially regulated by Golgin-97 mono-ADP-ribosylation by PARP12. This identifies a selective regulatory mechanism acting on the transport of Golgin-97– vs. Golgin-245–dependent cargoes. Of note, PARP12 enzymatic activity, and consequently Golgin-97 mono-ADP-ribosylation, depends on the activation of protein kinase D (PKD) at the TGN during traffic. PARP12 is directly phosphorylated by PKD, and this is essential to stimulate PARP12 catalytic activity. PARP12 is therefore a component of the PKD-driven regulatory cascade that selectively controls a major branch of the basolateral transport pathway. We propose that through this mechanism, PARP12 contributes to the maintenance of E-cadherin–mediated cell polarity and cell–cell junctions.

PARP12 | Golgin-97 ADP-ribosylation | PKD | intracellular membrane transport | E-cadherin

Adenosine diphosphate (ADP) ribosylation is a protein post-translational modification (PTM) consisting of the transfer of an ADP-ribose moiety from NAD^+ to target amino acids that is highly conserved throughout evolution (1–3). The enzymes catalyzing this reaction, named ADP-ribosyltransferases (ARTs), first diversified in bacteria into a variety of systems involved in defensive and offensive strategies in intragenomic, intergenomic, and intraorganismal conflicts, and have been acquired by eukaryotes from these conflict systems several times throughout evolution (1, 4). In eukaryotes, ADP-ribosyltransferases are often components of core regulatory and epigenetic processes (5–7). The analysis of their eukaryotic substrates is thus likely to provide information on the organization and regulation of key cellular functions.

The ARTs (8) constitute a major family of ADP-ribosyltransferases whose members catalyze ADP-ribosylation by adding either single or multiple units of the NAD^+-deriving ADP-ribose onto target proteins [respectively, mono- and poly-ADP-ribosylation, hereafter referred to as MARylation and PARylation (9)]. MARylation of mammalian proteins was first discovered decades ago to mediate the pathogenic action of bacterial toxins in host cells (10, 11). The endogenous occurrence of this PTM in mammalian cells later became evident (11–16) and, recently, with the definition of the different enzymes catalyzing the reaction, the cellular functions it regulates are emerging (17–19).

So far, eukaryotic ADP-ribosylation has been mainly studied under stress conditions, as exemplified by the role of poly (ADP-ribose) polymerase 1 (PARP1)–mediated PARylation during the DNA-damage response (20), PARP5, -12, and -13 in stress-granule formation (21–23), or PARP16 in the unfolded protein response (24, 25), while its impact on physiological cellular processes remains poorly defined.

Intracellular membrane transport is emerging as a function regulated by PARPs, with particular reference to Golgi-localized PARPs, namely PARP5 and -12 (26). PARP5 (also called tankyrase) is known to regulate the delivery of the glucose transporter GLUT4 from the *trans*-Golgi network (TGN) to glucose-storage vesicles and thus to the plasma membrane [PM (27–30)]. PARP12, originally described to be involved in defense against viral infections (31–34), is involved in the

Significance

Proteins are modified by many posttranslational modifications (PTMs) with crucial regulatory functions. A PTM attracting increasing interest is ADP-ribosylation, capable of altering crucial cellular targets. We show that mono-ADP-ribosylation by PARP12 of the protein Golgin-97 regulates transport to the plasma membrane of a specific group of functionally crucial cargo proteins. PARP12 is shown to be part of a regulatory cascade initiated by PKD and involving the direct phosphorylation and activation of PARP12. These events define, through Golgin-97 mono-ADP-ribosylation, a Golgi sorting mechanism for specific basolateral cargoes, including E-cadherin. Defects in this cascade impair E-cadherin transport and formation of cell–cell contacts, with potential consequences for the formation of adherens junctions, polarization of epithelial cells, and development of epithelial–mesenchymal transformation.

Author contributions: G.G. and D.C. designed research; G.G., A.F., L.S., M.L.M., R.D.M., M.P., and C.V. performed research; D.S. and A.R.B. contributed new reagents/analytic tools; G.G., A.F., M.L.M., R.D.M., S.P., A.L., C.V., and D.C. analyzed data; and G.G., A.L., and D.C. wrote the paper.

The authors declare no competing interest.

This article is a PNAS Direct Submission.

This article is distributed under Creative Commons Attribution-NonCommercial-NoDerivatives License 4.0 (CC BY-NC-ND).

[1]To whom correspondence may be addressed. Email: g.grimaldi@ieos.cnr.it, a.luini@ieos.cnr.it, c.valente@ieos.cnr.it, or daniela.corda@cnr.it.

This article contains supporting information online at http://www.pnas.org/lookup/suppl/doi:10.1073/pnas.2026494119/-/DCSupplemental.

Published December 30, 2021.

anterograde transport of the vesicular stomatitis virus G protein (VSVG) from the TGN to the PM (21, 26, 35) and is a well-known component of stress granules, where it translocates from the Golgi upon oxidative stress (21, 23).

The TGN is a major sorting station where cargoes are conveyed and sorted into distinct transport carriers for trafficking to post-Golgi compartments and to the PM (36). The different trafficking routes undertaken by individual cargoes are regulated by transport machineries, including small G proteins belonging to the ADP-ribosylation factor (Arf) and Rab families, cytosolic cargo-adaptor proteins, coat proteins, and accessory proteins, all involved in cargo "packaging" into specific transport carriers to achieve correct sorting and delivery (36–38).

Here, we report that PARP12 controls the basolateral transport of a subclass of basolateral cargoes, which includes VSVG and E-cadherin, through the MARylation of Golgin-97. Moreover, we find that PARP12-mediated MARylation requires the presence of protein kinase D (PKD), a master regulator of basolateral transport (39, 40), and that it is stimulated by PKD during cargo trafficking. Traffic-activated PKD phosphorylates PARP12, activating its enzymatic activity. It thus emerged that PARP12-mediated MARylation of Golgin-97 is a component of the PKD-dependent regulatory network underlying the basolateral secretion of a select subgroup of cargo proteins, including E-cadherin. Since E-cadherin is required for the formation of proper adherens junctions and epithelial polarization, we propose that the regulatory cascade described in this study may play a role in the maintenance of cellular polarity in epithelial cells and therefore in various body functions (41, 42).

Results

The Exocytosis of E-Cadherin Is Specifically Controlled by PARP12 and Golgin-97. We have previously reported that PARP12 is localized at the TGN, where it colocalizes with Golgin-97 (*SI Appendix*, Fig. S1) and supports the export of the basolateral cargo VSVG from the TGN to the PM (21). The exit of basolateral cargoes from the TGN occurs in different carriers, possibly exploiting different transport machineries (43). For instance, the exit of the VSVG cargo from the TGN occurs in carriers that require Golgin-97 (36, 44–46), and are similar to those used by the cargo E-cadherin and described by previous authors as tubulovesicular in shape (43), while other cargoes, exemplified by tumor necrosis factor alpha (TNFα), require Golgin-245 and use relatively smaller vesicular carriers to exit this compartment (43). To understand the role of PARP12 in regulating cargo exiting from the TGN, we analyzed its role in the export of these different basolateral cargoes, E-cadherin and TNFα, as examples of carrier segregation into the two distinct routes (43).

To this aim, we took advantage of the well-established synchronizable retention using selective hook (RUSH) transport system (43) to send synchronized waves of specific cargo proteins from the endoplasmic reticulum (ER), where they are synthesized, to the TGN. In most experiments, we used HeLa cells as a convenient model system that, although not fully polarized, maintains mechanisms for apical and basolateral cargo formation (47–49).

Cells, devoid or not of PARP12 expression, were transfected with SBP–EGFP (streptavidin binding protein–enhanced green fluorescent protein)–E-cadherin (Fig. 1*A*) or TNFα–SBP–EGFP (Fig. 1*B*) and the exit of cargoes from the TGN toward the PM was evaluated by quantifying the amount of cargo in the Golgi area after 60 min of biotin addition (Fig. 1 *C* and *D*). The transient depletion of PARP12 reduced the exit of E-cadherin from the TGN, as indicated by the entrapment of this cargo in the Golgi area (Fig. 1 *A* and *C*), while it did not affect the exocytosis of TNFα (Fig. 1 *B* and *D*).

To further evaluate the role of PARP12 in E-cadherin transport through the secretory pathway, the overall kinetics of SBP–EGFP–E-cadherin was then studied using confocal time-lapse imaging techniques in single living cells. Cells expressing SBP–EGFP–E-cadherin, and transiently depleted of PARP12 expression (by small interfering RNA [siRNA] treatment), were imaged for 2 h after exit from the ER (Fig. 1*E* and Movies S1 and S2), in order to follow synchronous waves of specific cargo populations. Normalized fluorescence intensities within the Golgi area (ROI, region of interest) were plotted as a function of time; values in Fig. 1*F* represent the Golgi distribution of E-cadherin during transport from the ER to the PM as a consequence of cargo influx from the ER into the Golgi and efflux toward the PM. Data show that, compared with control cells, the depletion of PARP12 did not affect cargo export out of the ER compartment (Fig. 1*F* and *SI Appendix*, Fig. S2), while it reduced cargo egress from the Golgi area (Fig. 1*F*), highlighting the selectivity of the role of PARP12 in E-cadherin transport from the Golgi to the PM.

In parallel, we assessed the specificity of Golgin-97 in E-cadherin exocytosis using previously characterized cells depleted of Golgin-97 by CRISPR-Cas9 technology [referred to as ΔGolgin-97 cells (50, 51)] or, as a negative control, depleted of Golgin-245 [ΔGolgin-245 cells (50)], and different cargo transport synchronization methods.

First, we simply expressed GFP–E-cadherin and monitored the arrival of this protein at the PM at a fixed time upon transfection (52). E-cadherin stained the PM and formed cell–cell junctions in both wild-type (WT) and ΔGolgin-245 cells, while the absence of Golgin-97 caused a defect in E-cadherin localization, with cargo trapped in the Golgi area and in intracellular vesicles. These structures colocalized with Rab11, suggesting that E-cadherin–containing transport carriers originate from a post-TGN/Rab11–positive compartment (*SI Appendix*, Fig. S3 *A* and *B*). By analyzing cells lacking Golgin-245, we could exclude a role of Golgin-245 in E-cadherin exocytosis. Curiously, this contrasts with the similarity of function between Golgin-97 and -245 as tethers in endosome-to-Golgi trafficking (50, 51, 53).

Second, we used the RUSH system, by which cargoes are first accumulated in the ER and then allowed to traverse the secretory pathway synchronously, and again evaluated the E-cadherin pool at the PM. The absence of Golgin-97 specifically reduced the arrival of E-cadherin at the PM (Fig. 1 *G* and *I*), while not affecting the transport of TNFα (Fig. 1 *H* and *J*), consistent with the above and with the PARP12 depletion data (Fig. 1 *A*–*D*). Instead, the absence of Golgin-245 specifically impaired TNFα transport, with no significant effect on E-cadherin arrival at the PM (Fig. 1 *I* and *J*). Along the same line, we examined the transport of VSVG, which depends on Golgin-97 and PARP12, like E-cadherin transport, using a well-characterized transport assay which relies on the thermosensitive mutant protein tsO45 from VSV (21, 45). Briefly, cells were infected with VSV and incubated at 40 °C to first accumulate the protein in the ER and then shifted to 20 °C, a temperature that allows the exit of the cargo proteins from the ER and the arrival at, but not the exit from, the TGN. The temperature was finally shifted to 32 °C, and transport from the TGN to the PM was monitored by immunofluorescence (*SI Appendix*, Fig. S4). Compared with WT cells, the absence of Golgin-97 increased the percentage of cells showing VSVG at the Golgi complex after 30 min of the temperature-block release (*SI Appendix*, Fig. S4), demonstrating a role of Golgin-97 in VSVG exocytosis.

Collectively, these data indicate that PARP12 and Golgin-97 are required for the exit of the basolateral cargoes VSVG and

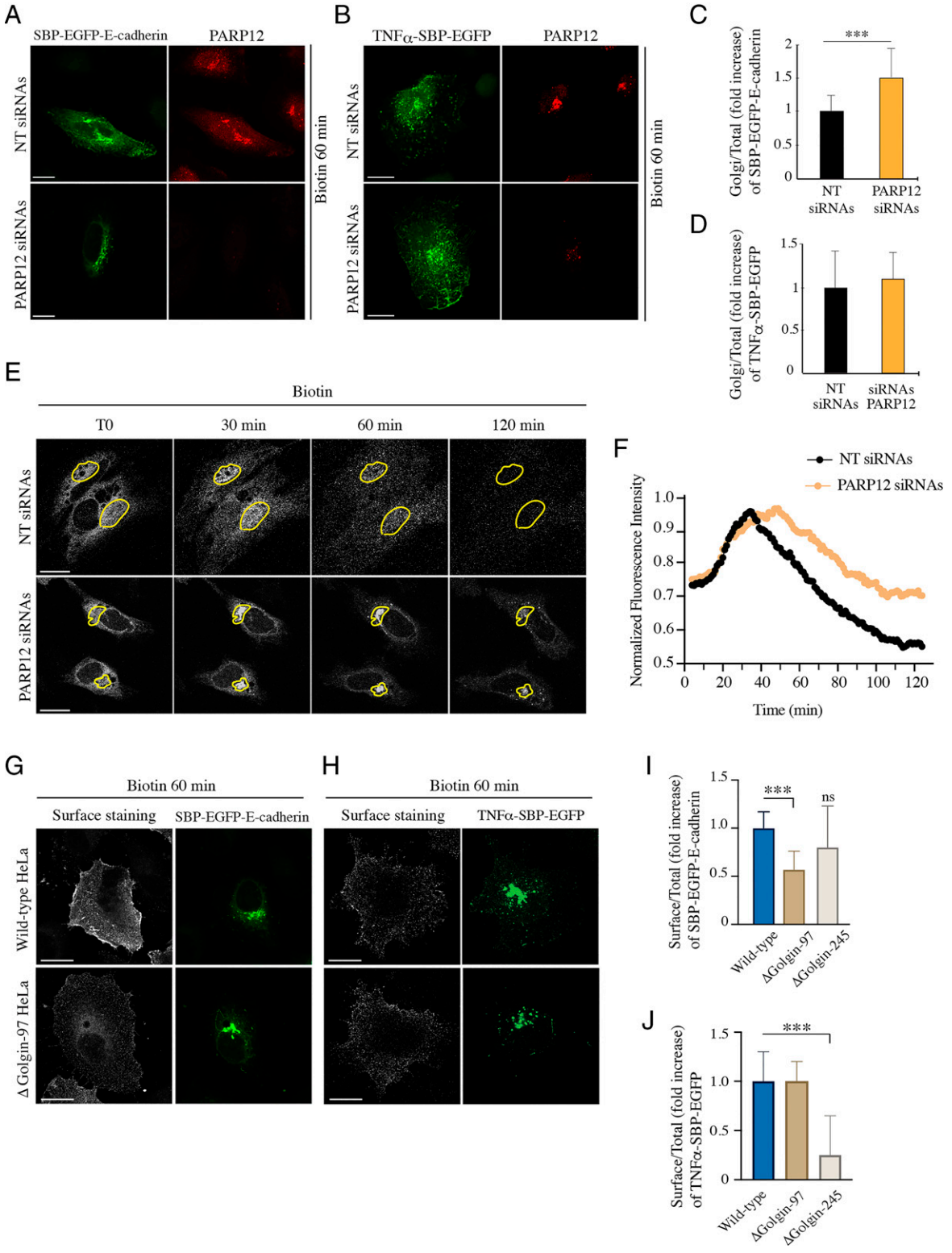

Fig. 1. Exocytosis of E-cadherin is specifically controlled by PARP12 and Golgin-97. (*A–D*) HeLa cells expressing the indicated RUSH-based constructs show an increased amount of EGFP–E-cadherin (*A*), but not EGFP–TNFα (*B*), at the Golgi complex after 60 min of biotin addition in the absence of PARP12. Quantifications are shown in *C* and *D*. (*E*) Cells expressing SBP–EGFP–E-cadherin and depleted or not of PARP12 expression were subjected to a biotin-based traffic pulse. Time-lapse confocal images were captured for 2 h at 1-min intervals. Shown are representative images at the designated times upon biotin addition (see the corresponding Movies S1 and S2). Yellow outlines mark the ROIs used for the analysis of time-based changes in Golgi fluorescence intensity. (*F*) Averaged and normalized time-based changes in fluorescence intensity of an ROI containing the Golgi complex are shown. Experimental data (filled circles) for each plot represent the average of nine cells. (*G–J*) Representative confocal images of the E-cadherin (*G*) or TNFα (*H*) pool at the PM (surface staining, gray) of synchronized RUSH-based E-cadherin/TNFα (green) in WT and ΔGolgin-97 cells; quantifications are reported in *I* and *J*. In the graphs are also reported the quantification of the E-cadherin and TNFα pool at the PM in ΔGolgin-245 cells. $n = 30$ cells from three different experiments, ±SD; $^{***}P < 0.001$, calculated by Student's *t* test; ns, not significant. (Scale bars, 10 μm.)

E-cadherin from the Golgi complex, possibly by synergically contributing to the assembly of specific trafficking machineries. Golgin-245 has no role in this transport event, while it is required for delivery of other cargoes, for example TNFα, to the PM.

Golgin-97 Is a PARP12 Substrate. The PARP12-mediated modulation of E-cadherin exocytosis (Fig. 1) might be due to PARP12-catalyzed modification of Golgin-97. To investigate this aspect, GFP-tagged E-cadherin localization was evaluated in WT cells treated with the general PARP inhibitor PJ34 (50 μM). This caused a mislocalization of E-cadherin that accumulated around the Golgi area in spots reminiscent of transport carriers (*SI Appendix*, Fig. S5*A*; no colocalization is observed with the Golgi marker GM130). In experiments on synchronized E-cadherin transport (using the RUSH system), PJ34 treatment delayed E-cadherin exit from the TGN and arrival at the PM (Fig. 2 *A* and *B*; live imaging results are shown in *SI Appendix*, Fig. S5*B* and Movies S3 and S4), and similar effects were observed upon PARP12 knockdown (Fig. 1 *A* and *C*), suggesting an involvement of PARP12 enzymatic activity in E-cadherin transport.

To further understand this aspect and considering the specificity of Golgin-97 in regulating E-cadherin transport, we evaluated if Golgin-97 could be a PARP12 substrate. We overexpressed Golgin-97 and analyzed the total cell lysates using the Af1521 *macro* domain–based pull-down assay, a well-characterized tool to specifically isolate ADP-ribosylated proteins (54, 55). We detected ADP-ribosylated Golgin-97 (Fig. 2*C*) but not Golgin-245 (used as control of specificity; *SI Appendix*, Fig. S6*A*), indicating that Golgin-97 was modified selectively under these experimental conditions (Fig. 2*C*). Golgin-97 MARylation was also analyzed after PARP12 depletion by which it was markedly reduced (Fig. 2*D*), indicating that Golgin-97 is a substrate of PARP12 activity. The potential contribution of PARP5 [also localized at the Golgi complex (27)] in this PTM was evaluated in cells treated for 2 h with PJ34 (50 μM) or with the PARP5-specific inhibitor IWR1 (25 μM): Golgin-97 was not MARylated in the presence of PJ34 while it was in the presence of IWR1, as expected, confirming the specificity of the PARP12-dependent modification (*SI Appendix*, Fig. S6*B*). In parallel, cells treated with the inhibitors were analyzed for E-cadherin transport. The IWR1 treatment did not alter E-cadherin arrival at the PM (*SI Appendix*, Fig. S6*C*), while PJ34 reduced it (Fig. 2 *A* and *B*), further corroborating the selective role of PARP12 in Golgin-97 MARylation and in E-cadherin transport.

Golgin-97 MARylation was then analyzed in in vitro assays, using purified full-length Golgin-97 and the PARP12 catalytic domain, in the presence of [^{32}P]NAD^{+}. Golgin-97 was modified under these conditions, indicating that it is a specific, direct substrate of PARP12-dependent MARylation (Fig. 2*E*).

In addition, and based on the colocalization between PARP12 and Golgin-97 at the TGN (*SI Appendix*, Fig. S1), we evaluated the interaction of the two proteins. To this end, total cell lysates overexpressing PARP12 were incubated with purified His–Golgin-97; His–Golgin-97 was then recovered and specifically eluted using imidazole. Fig. 2*F* shows that PARP12 interacted with Golgin-97 in a way that is dependent on Golgin-97 concentration.

With the aim of understanding if Golgin-97 MARylation is regulated during transport, this modification was analyzed during the RUSH-based E-cadherin transport assay. Cells were transiently transfected with the SBP–EGFP–E-cadherin construct and E-cadherin transport and Golgin-97 MARylation were followed at different time points during transport in the presence of cycloheximide (Fig. 3). A maximal Golgin-97 MARylation was observed at 20 to 30 min after release from the ER, when most cargo is at the TGN (and starts exiting this compartment), indicating that PARP12-mediated Golgin-97 MARylation is triggered by cargo in the TGN during a traffic wave. A different approach to investigate this aspect consisted of the synchronization of E-cadherin transport at different time points upon transfection (52). Cells were transfected with GFP–E-cadherin and Golgin-97 MARylation was detected at different time points (*SI Appendix*, Fig. S7*A*). Under these conditions, Golgin-97 MARylation resulted in being maximal when the cargo reached the Golgi complex and started exiting this compartment (*SI Appendix*, Fig. S7*A*). Finally, we analyzed Golgin-97 MARylation during the well-characterized VSVG traffic pulse in the presence of cycloheximide (*SI Appendix*, Fig. S7*B*). As shown in *SI Appendix*, Fig. S7*B*, MARylation of Golgin-97 was strongly activated at 20 °C, namely when cargo accumulates at the TGN, in line with the approaches described above. Of note, the increase in Golgin-97 MARylation was independent of the temperature shift, since in the absence of cargo no increase was detected at 20 °C, indicating that MARylation is triggered by the cargo and not by the 20 °C temperature (*SI Appendix*, Fig. S7*C*). The increase at 20 °C was followed by a drastic decrease of the MARylation signal when cargo exited the TGN at 32 °C, as expected. Curiously, there was an unexpected 30% rebound in the reaction rate at 60 min after the temperature shift (see *SI Appendix*, Fig. S7*B*, legend, for an interpretation of this phenomenon). Finally, in the absence of both VSVG and endogenous cargo, the signal at 20 °C was low and slightly increased at 32 °C, presumably reflecting the sensitivity of the basal (cargo-independent) reaction rate to temperature.

Altogether, these data demonstrate that Golgin-97 is specifically MARylated by PARP12 both in vitro and in intact cells; Golgin-97 MARylation is stimulated during membrane transport, and is essential for transport, consistent with a key role of its MARylation in the export and delivery of basolateral cargoes to the PM.

Identification of a Golgin-97–Modified Residue(s). Having defined Golgin-97 as a PARP12 substrate, we investigated the specific residue(s) targeted by this PTM. To this purpose and based on our previous data demonstrating that PARP12 modifies acidic residues (21), we exploited ADPredict, an in-house-developed bioinformatic tool for the prediction of the acidic residues (aspartic and glutamic acids, D and E) most prone to being MARylated (56). The predictions highlighted a few glutamic acid clusters (*SI Appendix*, Fig. S8 and Table S1) based on which we generated three separate multiple-point mutants, from here on addressed as Mut A: E381Q–E386Q–E393Q; Mut B: E558Q–E559Q–E565Q; and Mut C: E579Q–E585Q. Conservative mutations were introduced (exchanging acidic residues with their relative amide, E to Q) and the subcellular localization of the mutants was analyzed by immunofluorescence. All mutants localized at the TGN, similar to the WT protein (*SI Appendix*, Fig. S9*A*). This was examined after nocodazole-induced disruption (33 μM for 3 h) of the Golgi ribbon into smaller structures, "ministacks" (*SI Appendix*, Fig. S9*B*), which are often used to precisely determine protein localization across Golgi stacks (57).

The identified residues locate in the coiled-coil domain of Golgin-97 (residues 50 to 657). We assessed the possible effect of each mutant on the coiled-coil stability, using the online tool Multicoil2 (58). In no cases was the peculiar hydrophobic interaction crucial for coiled-coil folding perturbed; the minor changes introduced never significantly appeared to affect the availability of the coiled-coil structure for possible protein–protein interactions (*SI Appendix*, Table S2).

Next, we tested the generated Golgin-97 mutants for their MARylation levels. Based on the findings that MARylation of Golgin-97 was activated during protein transport stimulation (Fig. 3 and *SI Appendix*, Fig. S7), we analyzed MARylation of

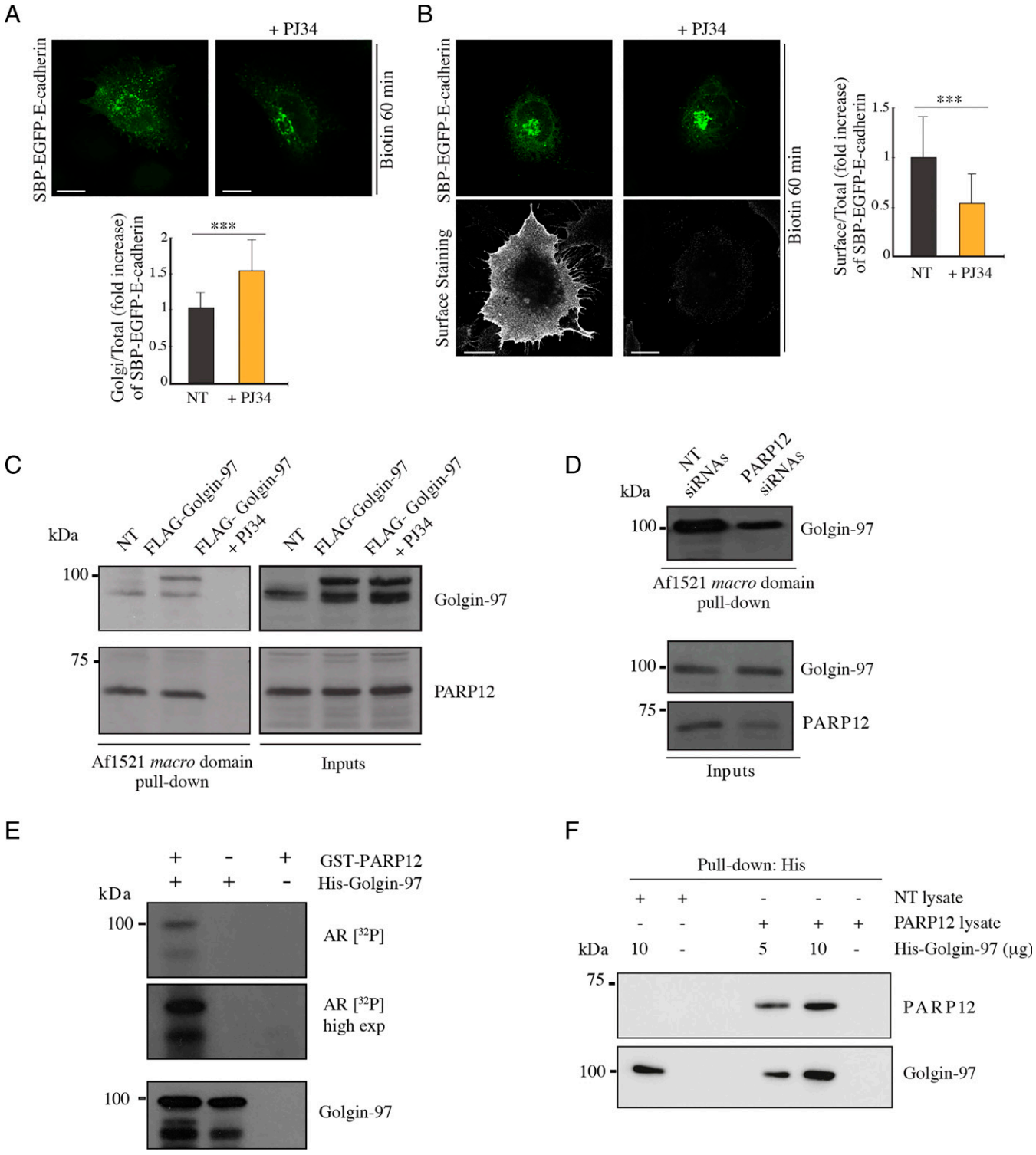

Fig. 2. Golgin-97 is a PARP12 substrate. (*A* and *B*) Representative confocal images of (*A*) SBP–EGFP–E-cadherin (green) or (*B*) its pool at the PM (surface staining, gray) in cells treated or not with PJ34 (50 μM, 2 h). Graphs show quantification of E-cadherin at the Golgi complex or at the PM. (*C* and *D*) Af1521 *macro* domain–based pull-down assay of total cell lysates obtained from (*C*) cells transfected or not (NT) with FLAG-tagged Golgin-97 and treated with the PARP inhibitor PJ34 (50 μM, 2 h), or (*D*) cells depleted of PARP12 or not, showing the PARP12-dependent MARylation of Golgin-97. PARP12 was detected as an internal control. (*E*) In vitro MARylation assay using a GST-tagged purified PARP12 catalytic fragment and His-tagged purified Golgin-97, in the presence of [^{32}P]NAD$^+$, detected by autoradiography (AR [^{32}P]). (*E*, *Bottom*) Total levels of Golgin-97. (*F*) In vitro pull-down assay of His–Golgin-97 incubated with cell lysates overexpressing or not PARP12 (NT lysate vs. PARP12 lysate), and eluted with an imidazole-containing buffer. The samples were subjected to sodium dodecyl sulfate–polyacrylamide gel electrophoresis and Western-blotting analysis, as indicated. n = 30 cells from three different experiments, ±SD; ***$P < 0.001$, calculated by Student's t test. (Scale bars, 10 μm.)

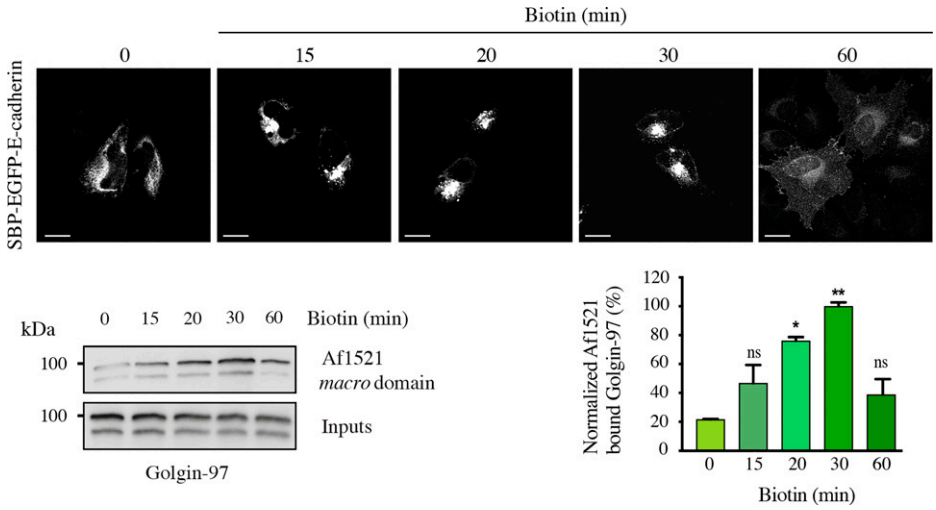

Fig. 3. MARylation of Golgin-97 is triggered during transport. Representative confocal images of SBP–EGFP–E-cadherin localization during traffic-pulse experiments at different times, as indicated. MARylation levels of Golgin-97 during transport were analyzed using an Af1521 *macro* domain–based pull-down assay of total cell lysates obtained from HeLa cells subjected to a RUSH-based E-cadherin transport for different times. Blots are representative of three independent experiments. Quantifications ± SD are reported in the graphs. *$P < 0.05$, **$P < 0.01$, calculated by Student's t test. (Scale bars, 10 μm.)

Golgin-97 mutants under a VSVG traffic pulse, again using the Af1521 *macro* domain–based pull-down assay. The MARylation of Mut B was almost abolished, while Mut A and Mut C showed a clear residual MARylation, corresponding approximately to 50% of WT Golgin-97 MARylation (Fig. 4). This indicates that the glutamic cluster 558–559–565 (mutated in B, but still present in the other two mutants) is the only one to be quickly and efficiently MARylated during the transport pulse and that is therefore probably the crucial one for transport (see below). In support of these data, when the MARylation of Golgin-97 and its mutants was analyzed under steady-state or in vitro assay conditions (*SI Appendix*, Fig. S10), we observed a low MARylation of the WT Golgin-97 itself and, consequently, an almost complete abolishment of MARylation for the mutants.

Collectively, these data indicate that Golgin-97 MARylation specifically occurs during protein transport and identify residues 558–559–565 (mutated in B) as those relevant to this process.

MARylated Golgin-97 Is Required for Basolateral Export of E-Cadherin. To assess the significance of MARylation in the export of E-cadherin, GFP-tagged E-cadherin localization was evaluated in ΔGolgin-97 cells and transfected with the WT Golgin-97 or with its ADP-ribosylation–defective mutants. Transfected WT Golgin-97 rescued the localization defect observed in ΔGolgin-97 cells, resulting in a clear PM localization of E-cadherin. Notably, the distribution of E-cadherin to the PM was typical of the morphology of the adherens junctions (*SI Appendix*, Fig. S11*A*). Mut B was unable to recover the defective phenotype, and showed the same accumulation of GFP-tagged E-cadherin in perinuclear carriers as observed in ΔGolgin-97 cells (*SI Appendix*, Figs. S3 and S11*A*), while Mut A and Mut C recovered the defect as well as WT Golgin-97 (*SI Appendix*, Fig. S11*A*), with formation of the adherens junction phenotype.

These results were substantiated by monitoring the GFP-tagged E-cadherin transport in live imaging experiments performed in ΔGolgin-97 HeLa cells transiently transfected with the WT Golgin-97 or with its ADP-ribosylation–defective Mut B, which again was unable to rescue the E-cadherin transport, as reported above (*SI Appendix*, Fig. S11*B* and Movies S5, S6, S7, and S8).

The role of Golgin-97 MARylation in E-cadherin transport was further characterized by analyzing the overall cargo kinetics in single-cell live imaging experiments (as described above for PARP12 depletion). To this purpose, ΔGolgin-97 HeLa cells were cotransfected with SBP–EGFP–E-cadherin and WT Golgin-97 or its ADP-ribosylation–defective mutants and E-cadherin transport was imaged for 2 h after exit from the ER (Fig. 5, *SI Appendix*, Figs. S12 and S13, and Movies S9, S10, S11, S12, and S13). Changes in E-cadherin distribution along the secretory pathway were represented as the normalized fluorescence intensities in the Golgi region as a function of time (Fig. 5*A* and *SI Appendix*, Fig. S13*A*). These transport kinetics showed that the expression of WT Golgin-97 in ΔGolgin-97 cells recovered the delay in cargo exit from the Golgi area caused by Golgin-97 absence. Mut A and Mut C rescued cargo egress from the Golgi nearly as efficiently as WT Golgin-97 (Fig. 5), while the expression of Mut B was unable to rescue cargo export from the Golgi area, indicating that the glutamic acid cluster in positions 558–559–565 is the one relevant for the role of Golgin-97 in TGN export, as also supported by the data on the MARylation of the mutants (see above and Fig. 4). ER-to-Golgi transport was not altered in any of the aforementioned conditions, except for Mut A, which led to an apparently faster ER-to-Golgi transport (*SI Appendix*, Fig. S13*B*). However, this effect is not expected to contribute to the delay in arrival at the PM, and thus was not explored further.

Similar results were obtained by analyzing the E-cadherin pool at the PM. ΔGolgin-97 cells were cotransfected with SBP–EGFP–E-cadherin and WT Golgin-97 or its ADP-ribosylation–defective mutants and E-cadherin labeling at the PM was analyzed by performing E-cadherin surface staining at different time points, as indicated (*SI Appendix*, Fig. S14*A*). Compared with ΔGolgin-97 cells, only the overexpression of WT Golgin-97 fully recovered the arrival of E-cadherin at the PM; Mut A and Mut C showed instead a similar or slightly slower recovery, while overexpression of Mut B was unable to recover the defect observed in the absence of Golgin-97 (*SI Appendix*, Fig. S14*A*).

Of note, the defective MARylation in Golgin-97 did not change its colocalization with the cargo E-cadherin at the Golgi level, as demonstrated by the colocalization analysis between E-cadherin and Golgin-97 WT or its ADP-ribosylation–defective

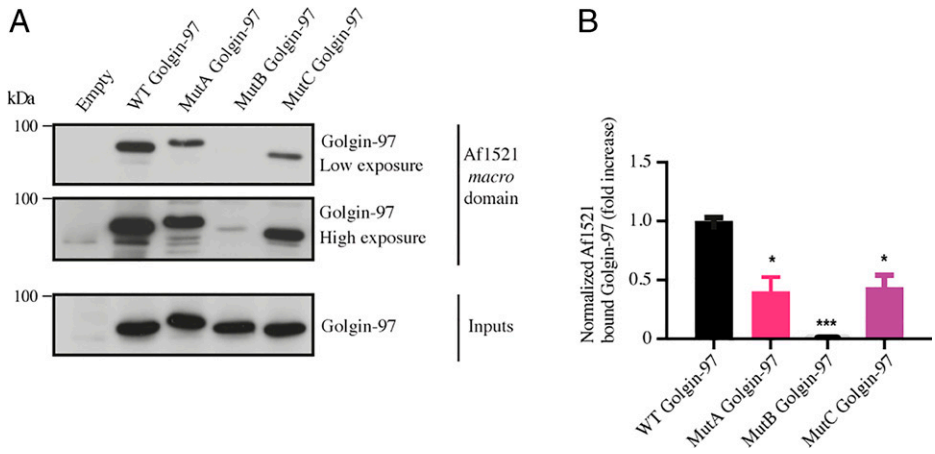

Fig. 4. Validation of Golgin-97 MARylation-defective mutants in cells subjected to a traffic pulse. (*A*) Af1521 *macro* domain–based pull-down assay of total lysates obtained from cells transfected with the full-length Golgin-97 or with its mutants and subjected to a VSVG traffic pulse. MARylation levels of Golgin-97 during transport were analyzed using an Af1521 *macro* domain–based pull-down assay. The bound proteins were eluted and detected by Western blotting with an anti–Golgin-97 antibody. (*B*) Quantifications ± SD of MARylatedGolgin-97. *$P < 0.05$, ***$P < 0.001$, calculated by Student's *t* test.

mutants (*SI Appendix*, Fig. S14 *B* and *C*). From this point on, we only used Mut B for further experiments.

Prompted by the above data, we analyzed the role of MARylation in the interaction with functionally relevant proteins. FIP1/RCP is a well-characterized direct interactor of Golgin-97 required for tethering and fusion of recycling endosome (RE)–derived retrograde transport vesicles to the TGN (59) and in transport from the RE to the PM (60).

We evaluated if the mutations introduced in Golgin-97 would modulate its interaction with FIP1/RCP. Cells were cotransfected with Myc/FLAG-tagged FIP1/RCP and tomato-tagged Golgin-97 WT or its ADP-ribosylation–defective mutant; FIP1/RCP was immunoprecipitated and the interaction with Golgin-97 was evaluated using a Golgin-97 antibody. The results show that WT Golgin-97 interacted with FIP1/RCP, as expected, and that Mut B increased the interaction with FIP1/RCP (Fig. 5*D*), suggesting that MARylation is involved in the disassembling of dynamic Golgin-97 complexes (*Discussion*).

Next, we examined the effects of Golgin-97 on specific traffic steps from the Golgi complex. Compared with control cells, ΔGolgin-97 cells showed longer, larger, and more abundant tubular carriers containing E-cadherin that were apparently unable to distance themselves from the Golgi. This phenotype was reverted by the overexpression of WT Golgin-97, but not by the ADP-ribosylation–defective Mut B (*SI Appendix*, Fig. S14 *D–F*).

Collectively, these results support the requirement of Golgin-97 MARylation in controlling E-cadherin exit from the Golgi area, formation and fission of carriers, and thus a correct cargo delivery to the PM.

Golgin-97 MARylation Regulates Adherens Junctions in MCF7 Cells. The relevance of PARP12 activity in E-cadherin exocytosis was further substantiated by evaluating E-cadherin localization in epithelial MCF7 cells, which endogenously express E-cadherin, by immunofluorescence. The monolayer of control MCF7 cells showed a major distribution of E-cadherin to the PM and evident images of adherens junctions.

In PARP12-depleted cells, E-cadherin was instead mostly retained in the Golgi area, with scarce E-cadherin staining at the PM and no images of adherens junctions (Fig. 6*A*). Labeling of calnexin, which did not show any colocalization with E-cadherin, was performed to exclude a possible retention of the protein at the ER level (*SI Appendix*, Fig. S15*A*). A similar phenotype was observed in MCF7 cells transiently depleted of Golgin-97 (*SI Appendix*, Fig. S15*B*).

In these cells, we have also directly evaluated MARylation of endogenous Golgin-97 again using the Af1521 *macro* domain–based pull-down assay from total lysates of control cells at steady state, or of cells depleted of PARP12 or treated with the PARP inhibitor PJ34. MARylation was strongly reduced both in the absence of PARP12 and when the PARP catalytic activity was inhibited. These findings are in full agreement with and support the data on E-cadherin localization reported above, in that they show the requirement of the Golgin-97 modification for an E-cadherin localization at the PM and for adherens junction formation (Fig. 6*A*). Thus, endogenously expressed E-cadherin behaves as the protein expressed in HeLa cells, reinforcing the conclusion that PARP12-mediated MARylation of Golgin-97 controls a correct transport of E-cadherin toward the PM.

PARP12-Mediated MARylation of Golgin-97 Is under the Control of PKD Activity. The export of basolateral cargoes at the TGN is regulated by signaling pathways, with PKD-dependent signaling being one of the most important regulatory pathways at the TGN (39, 40, 61). As reported, basolateral cargoes trigger a signaling pathway at the TGN that results in PKD recruitment and activation, followed by PKD-mediated phosphorylation of several substrates needed for a correct delivery of carriers to the basolateral PM, such as PI4KIIIβ (39). Based on this knowledge and on the increase of Golgin-97 MARylation during basolateral cargo pulses (Fig. 3 and *SI Appendix*, Fig. S7), we evaluated if PARP12-mediated Golgin-97 MARylation occurs downstream of PKD signaling. To this end, MCF7 cells were treated with the PKD inhibitor CRT0066101 (10 μM, 2 h) and Golgin-97 MARylation was evaluated by using the Af1521 *macro* domain–based pull-down assay. As shown in Fig. 6*C*, inhibition of PKD activity almost abolished Golgin-97 MARylation, indicating that this is a PKD-dependent event. Similar results were obtained in cells transiently depleted of PKD1, PKD2, or both (Fig. 6*D* and *SI Appendix*, Fig. S15*C*).

These data led us to test whether PARP12 could be a PKD substrate. In vitro kinase assays were performed using purified GST (glutathione S-transferase)–PKD1 or its kinase-dead (KD) mutant, used as control (Fig. 6*E*), and a PARP12 catalytic fragment. The phosphorylation status of PARP12 was then detected using a characterized antibody (Fig. 6*E*). Similar experiments were carried out using Myc-tagged PARP12 immunoprecipitated from cell lysates (*SI Appendix*, Fig. S16). The data demonstrate that PARP12 is a substrate of PKD.

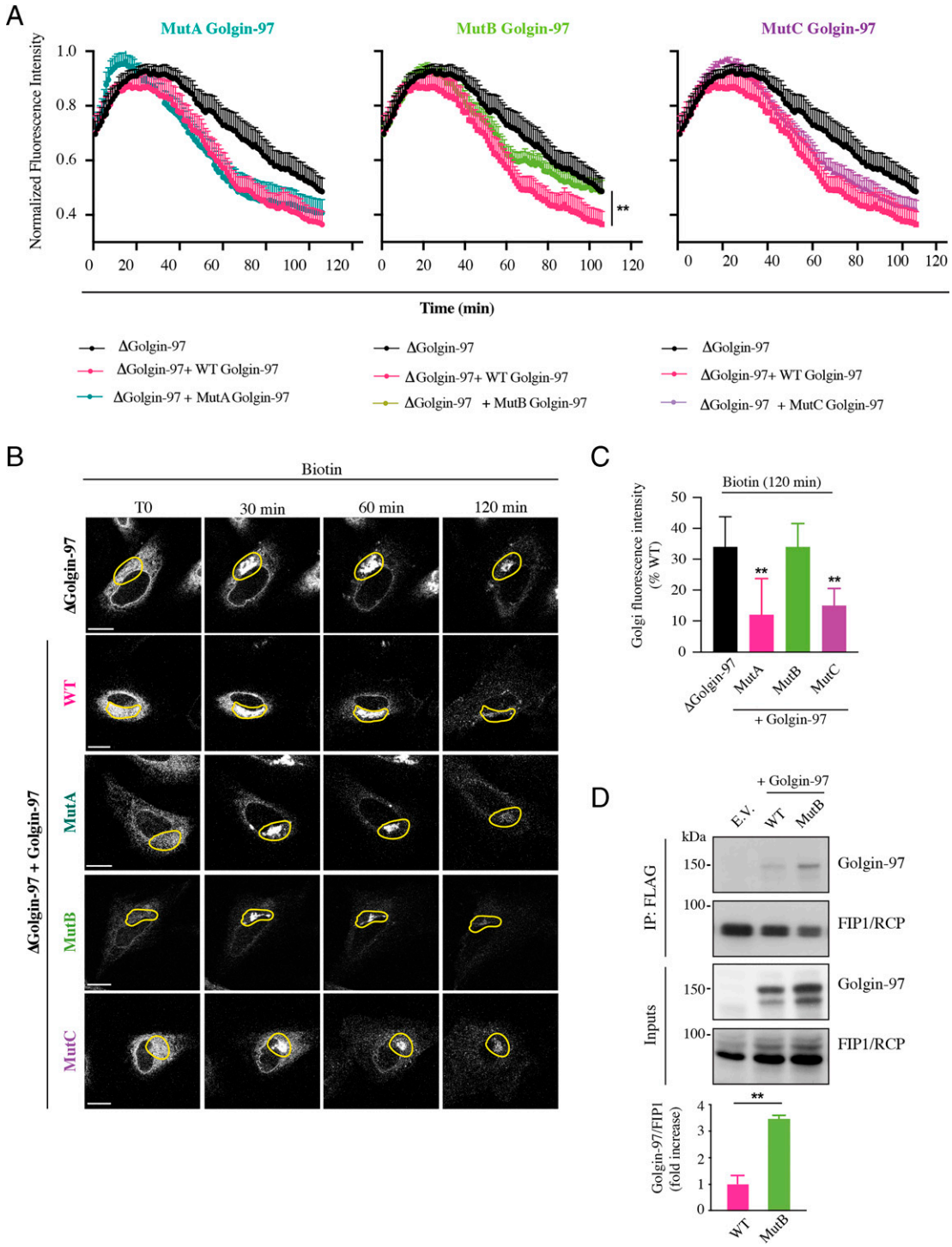

Fig. 5. Functional analysis of Golgin-97 MARylation-defective mutants in E-cadherin transport. ΔGolgin-97 HeLa cells expressing SBP–EGFP–E-cadherin alone or in combination with tomato-tagged WT Golgin-97 or its mutants (Mut A, Mut B, and Mut C) were subjected to a biotin-based traffic pulse. Time-lapse confocal images were captured for 2 h at 1-min intervals. (*A*) Averaged (with SEM) and normalized time-based changes in fluorescence intensity of an ROI containing the Golgi complex are shown for all the indicated conditions. Experimental data for each plot represent the average of nine cells. Values reported in the graph were plotted starting from the same fluorescence value for each condition. Corresponding single kinetics are reported in *SI Appendix*, Fig. S13. The recovery provided by the overexpression of WT Golgin-97 is statistically significant (**$P < 0.01$) compared with that due to its ADP-ribosylation–defective Mut B. (*B*) Representative frames of time-lapse E-cadherin transport at the indicated times upon biotin addition in ΔGolgin-97 HeLa cells expressing SBP–EGFP–E-cadherin alone or in combination with tomato-tagged WT Golgin-97 or its mutants. See the corresponding Movies S9, S10, S11, S12, and S13. Yellow outlines mark the ROIs used for the analysis of time-based changes in Golgi fluorescence intensities reported in *A*. (Scale bars, 10 μm.) (*C*) Quantification of the E-cadherin fluorescence intensity at the Golgi complex (relative to cells used for quantification of time-lapse experiments) after 120 min of biotin addition in the different Golgin-97 overexpression conditions, as indicated. (*D*) Immunoprecipitation of FLAG-tagged FIP1/RCP from total lysates obtained from cells cotransfected with tomato-tagged Golgin-97 (WT or Mut B). The bound proteins were eluted and detected by Western blotting, as indicated. E.V., empty vector; IP, immunoprecipitation. Quantifications ± SD are reported in the graph. **$P < 0.01$, calculated by Student's *t* test.

Moreover, we found that PARP12 phosphorylation increases its catalytic activity, as evaluated by monitoring in vitro Golgin-97 MARylation upon PARP12 phosphorylation by PKD1 (Fig. 6*F*). These results are in line with the absence of Golgin-97 MARylation upon PKD inhibition observed in MCF7 cells (Fig. 6*C*) and demonstrate that PKD-mediated phosphorylation is required for the activation of PARP12 at the TGN; activated PARP12 can then MARylate Golgin-97 and support basolateral cargo export. As a proof of concept, MCF7 cells were treated with the inhibitor CRT0066101 and analyzed by immunofluorescence to follow E-cadherin localization. Inhibition of PKD catalytic activity caused a loss of E-cadherin from the PM and a consequent impairment in the formation of adherens junctions (*SI Appendix*, Fig. S15*D*). This phenotype recalls the phenotype observed upon PARP12 or Golgin-97 depletion in MCF7 cells (Fig. 6*A* and *SI Appendix*, Fig. S15*B*), further corroborating the finding that PARP12-mediated MARylation occurs downstream of and requires PKD activation, and is therefore part of the PKD signaling cascade acting at the TGN.

As a whole, this set of data demonstrates that the PARP12-mediated addition of ADP-ribose onto specific E residues of Golgin-97 controls the correct trafficking of the cargo E-cadherin, facilitating its exit from the Golgi complex (by contributing to carrier fission) and correct delivery in appropriate basolateral transport carriers, and that this is part of the more general PKD-mediated signaling acting at the TGN.

Discussion

In this study, we demonstrate that the ADP-ribosyltransferase PARP12 catalyzes the MARylation of Golgin-97, and that this modification is required for selectively supporting the formation of tubulovesicular carriers that originate from the TGN; these tubular structures carry a subclass of cargo basolateral proteins which includes E-cadherin and VSVG to the PM and specifically to the adherens junctions, where E-cadherin participates in their assembly. In addition, we show that this process is fully integrated in the mechanism of basolateral membrane traffic controlled by PKD, in that PARP12 is a direct substrate of this kinase, and that this modification controls its ADP-ribosyltransferase activity, hence controlling Golgin-97 MARylation. This makes PARP12-driven MARylation and its target Golgin-97 significant players in the regulation of TGN exit and sorting, a critical step in intracellular membrane transport in epithelia.

Golgins are a large and heterogeneous family of long coiled-coil proteins associated with different compartments of the Golgi complex (62, 63). As a family, Golgins are ubiquitous and highly conserved in evolution and play a variety of roles in membrane trafficking, whose functional significance and molecular mechanisms have been gradually emerging over the last decade. Golgin-97 is part of a subgroup of Golgins (Golgin-97, Golgin-245/230, GCC88, and GCC185) characterized by a GRIP domain, a sequence of about 50 to 60 amino acids at their C terminus (64, 65). The binding between the GRIP domain of Golgin-97, Golgin-245, and GCC88 and the small GTPase Arl1 determines their localization at the TGN (62, 66, 67). In the case of GCC185, two small GTPases, Rab6 and Arl1, have been proposed to determine its localization at the TGN (68, 69).

From a functional standpoint, Golgin-97 and other TGN Golgins were first reported to operate in retrograde transport between endosomes and the TGN (62, 63, 70). In addition, and directly relevant to the current study, some TGN Golgins have also been described to be involved in the formation of post-Golgi carriers and in the transport of specific cargo proteins to the PM (52, 71, 72). These two roles of the Golgins might be functionally interconnected through retrograde transport–mediated recovery at the TGN of machinery proteins necessary for subsequent rounds of antegrade export (73, 74).

Golgin-97 and Golgin-245 have been demonstrated to be involved in the transport of different basolateral cargoes (51, 53). Golgin-97 has been shown to specifically act in the transport of large tubulovesicular carriers containing E-cadherin from the TGN to the PM, through a route that includes Rab11-containing endosomes (52, 75); moreover, Golgin-97 has recently been shown to control the export of the potassium channel Kir2.1 to the basolateral PM by directly interacting with the channel, and possibly facilitating the formation of the AP1 export carrier required for this traffic step (72). Golgin-245 controls the transport of smaller vesicular carriers containing TNFα (71).

These findings are part of an emerging scenario in which multiple exit routes operate from the Golgi to the PM and to endolysosomes, and need to be selectively regulated to prevent missorting and mistargeting of cargoes (76–78). Our data show that the two types of carriers, which are most likely responsible for transporting the bulk of the basolateral proteins to the PM (altogether over a thousand), are differentially regulated by the selective MARylation of Golgin-97 by PARP12 in that this specific modification selectively supports the transport of large tubular basolateral cargoes that carry E-cadherin, apparently by supporting their fission and progression from the RE to the PM, while it has no effect on TNFα-containing carriers.

The Golgin-97 MARylation reaction that is relevant for traffic appears to occur selectively on the three glutamic acids 558–559–565 in the Golgin-97 coiled-coil domain, initially identified using a bioinformatics tool developed in our laboratory [ADPredict (56)]. Notably, Golgin-97 MARylation also regulates its interaction with FIP1/RCP, and thus likely with Rab11, possibly contributing to the dynamics of a protein complex relevant to transport. A detailed characterization of the mechanisms by which PARP12-catalyzed MARylation could regulate this anterograde transport is ongoing.

From a functional standpoint, the main aspect emerging from our data, namely the cargo specificity provided by the PARP12-mediated MARylation of Golgin-97 during exocytosis, can be interpreted in the context of the growing evidence that various types of molecular machineries for cargo export operate between the TGN and the PM. In addition to the above two morphologically distinct carriers, namely tubular or vesicular-like post-Golgi carriers, which probably correspond to different mechanisms for segregation of the cargoes both intra- and post-Golgi (43), other carriers have been described that specifically export some proteins but not others, for example the CARTS [carriers of the TGN to the cell surface (79, 80)]. Similarly, it has been proposed that cargo segregation occurs also during export of endolysosomal proteins out of the TGN, where two post-Golgi carrier populations, namely tubular carriers for transferrin receptor and LAMP1 (which also contain VSVG when cotransported) and vesicular carriers for cationic-dependent mannose-6-phosphate receptor, have been described (81). The significance of this variety of transport pathways leaving the TGN despite its functional importance remains to be clarified; it is probable that one of the functions of this multiplicity is that different cargo classes can be regulated differently and targeted to different PM subdomains, for example those targeted by E-cadherin to facilitate its clustering and thus adherens junction extension and maturation.

The selective regulation of Golgin-97–dependent carriers reported in this study represents an intriguing example of regulation of a specific type of carrier and therefore of the transport of a specific group of cargo proteins toward the basolateral PM. The functional role of this type of selective regulation is likely to emerge from the analysis of PARP12-dependent MARylation and of the type of cargoes this MARylation supports.

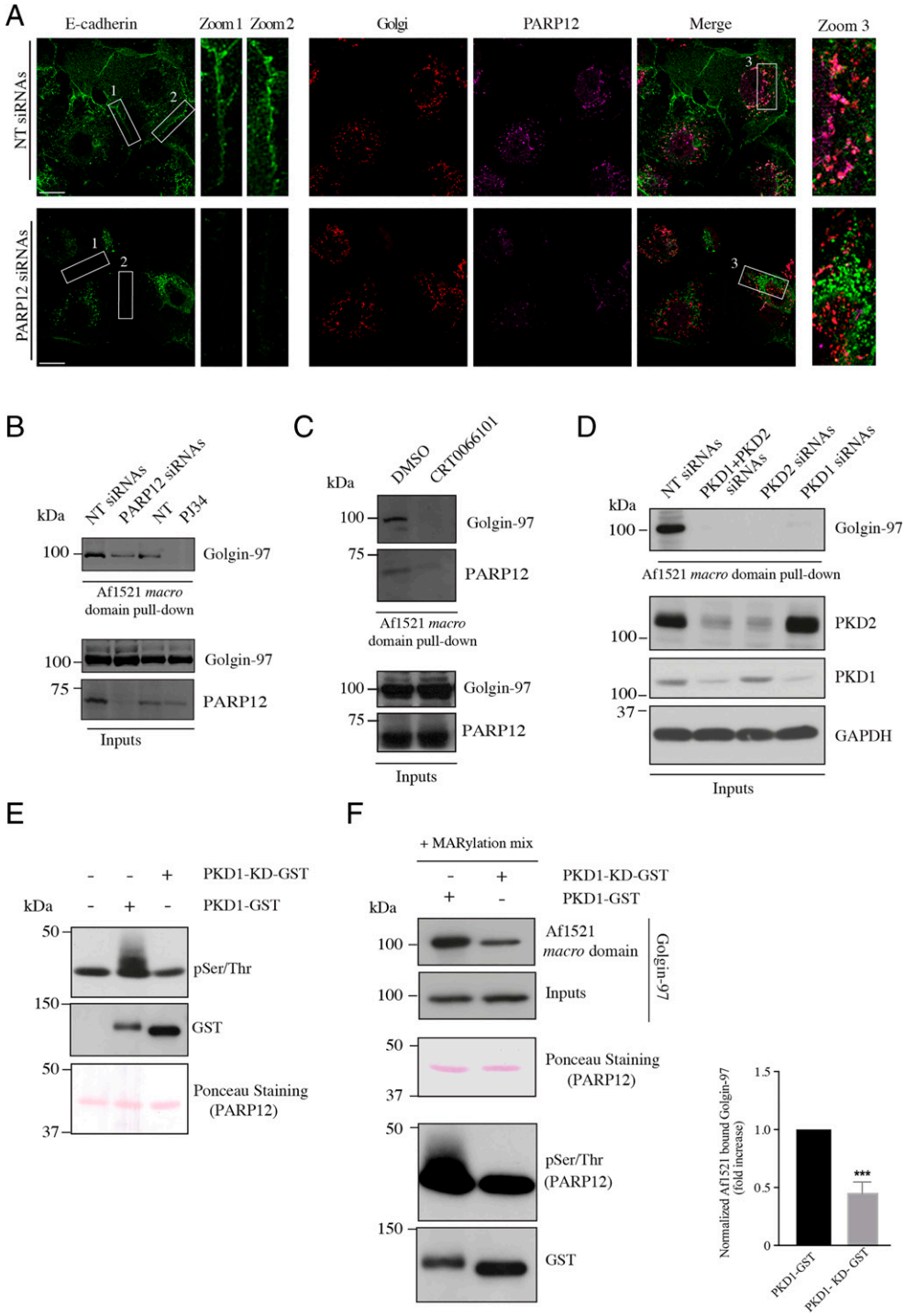

Fig. 6. PARP12-driven Golgin-97 MARylation and PKD activity regulate the localization of endogenous E-cadherin in MCF7. (*A*) Representative confocal images of MCF7 cells depleted of PARP12 or not and stained for endogenous E-cadherin (green), Golgin-245 (red; used as a TGN marker), and PARP12 (magenta). Zoom 1 and 2: enlarged views of E-cadherin signal at the PM, where E-cadherin forms adherens junctions. Zoom 3: enlarged views of E-cadherin signal at the Golgi area. (Scale bars, 10 μm.) (*B*) Af1521 *macro* domain–based pull-down assay of total lysates obtained from MCF7 cells depleted of PARP12 or not, and from MCF7 untreated (NT) or treated with PJ34 (50 μM, 2 h) showing the PARP12-dependent MARylation of Golgin-97. (*C* and *D*) Af1521 *macro* domain–based pull-down assay of total lysates obtained from (*C*) MCF7 cells treated or not (dimethyl sulfoxide; DMSO) with the PKD inhibitor (CRT0066101, 10 μM, 2 h) or (*D*) depleted or not of PKD1, PKD2, or both, showing the PKD dependence of PARP12-mediated MARylation of Golgin-97. Glyceraldehyde 3-phosphate dehydrogenase (GAPDH) was used as loading control. Relative quantifications are reported in *SI Appendix*, Fig. S15*C*. (*E*) In vitro kinase assays using a purified PARP12 catalytic fragment and GST–PKD1 or its dead mutant (PKD1–KD–GST). Phosphorylated proteins were detected using an anti–phospho-Ser/Thr antibody. Levels of PARP12 and PKD1 were controlled by Ponceau staining or by Western blotting using an anti-GST antibody, respectively. Results shown are representative of three independent experiments. (*F*) In vitro MARylation assay using His-tagged purified Golgin-97 and a purified PARP12 catalytic fragment, previously phosphorylated by PKD1. The MARylation assay was followed by an Af1521 *macro* domain–based pull-down assay to recover the pool. Bound proteins were eluted and detected by Western blotting with an anti–Golgin-97 antibody. Total levels of a PARP12 catalytic fragment and PKD1 were monitored by Ponceau staining or by Western blotting using an anti-GST antibody, respectively. ***$P < 0.001$, calculated by Student's *t* test.

Relevant in this regard is that Golgin-97 MARylation is under the control of PKD. PKD is a master regulator of TGN function that is activated and recruited from the cytosol to the TGN in a diacylglycerol-dependent manner (61) during the passage of cargo through the TGN, and mediates the formation of basolateral carriers containing VSVG and E-cadherin (48). From this study, PARP12 emerges as a substrate of PKD that regulates PARP12 catalytic activity at the TGN through phosphorylation. The consequent Golgin-97 MARylation appears therefore to be a crucial node in the regulatory network of TGN export and sorting.

E-cadherin plays a central role in epithelial polarity (41, 82). In this context, MARylated Golgin-97 is required to support a correct export and targeting of E-cadherin–containing carriers to the appropriate PM domain. E-cadherin mediates the formation of adherens junctions, required to maintain an intact architecture of the normal epithelium (83). A crucial event in tumoral transformation is the loss of adherens junctions and thus of cell polarity, while gaining migratory and invasive properties, an event known as epithelial-to-mesenchymal transition [EMT (82)]. An altered trafficking of E-cadherin impinges on the stability of the adherens junctions, as already reported for defective endosomal trafficking of E-cadherin (84). The present work places Golgin-97 MARylation as a regulator of E-cadherin exocytosis, an event with consequences for cell–cell junction stability. We envision that a hampered Golgin-97 MARylation, associated with defective E-cadherin transport, could contribute to the loss of adherens junctions and polarity. Considering the role of E-cadherin and EMT in tumor spreading, PARP12-mediated MARylation of Golgin-97 may play a significant role in EMT and metastasis processes.

Materials and Methods

Molecular cloning procedures, cell-culture conditions, and sources and dilution of antibodies and reagents used can be found in *SI Appendix*.

Transient Transfections and siRNA-Mediated Knockdown. Cells were transfected with the indicated plasmids or with siRNA oligos using TransIT-LT1 reagent or Lipofectamine RNAiMAX, respectively, according to the manufacturer's instructions. Details are reported in *SI Appendix*.

In Vitro ADP-Ribosylation and Kinase Assays. The ADP-ribosylation assay and the kinase reaction were performed as previously described (21, 39), with some modifications (*SI Appendix*). Where indicated, phosphorylated PARP12 was then used in in vitro MARylation assays in the presence of His-tagged Golgin-97.

Purification of His-Tagged Golgin-97 and His Pull-Down Assay. His-tagged Golgin-97 (WT and its mutants) was purified as detailed in *SI Appendix*. Histidine pull-down assays were carried out as previously described (46), with some modifications, and described in *SI Appendix*.

***Macro* Domain–Based Pull-Down Assay.** Purification of the Af1521 *macro* domain and the procedure for the pull-down assay were described previously (55) and detailed in *SI Appendix*.

Immunofluorescence and Confocal Microscopy. Immunofluorescence, VSVG, or RUSH-based assays were performed as previously described (21, 43, 45). Detailed procedures and relative quantification methods are described in *SI Appendix*.

Statistical Analysis. *P* values were calculated comparing the control and each treated group individually using Student's *t* test. All statistical parameters are listed in the corresponding figure legends.

Data Availability. All study data are included in the article and supporting information.

ACKNOWLEDGMENTS. We thank Drs. S. Munro and J. J. H. Shin (Medical Research Council Laboratory of Molecular Biology, Cambridge, United Kingdom) for providing ΔGolgin-97, ΔGolgin-245, and the parental cell lines; Dr. P. Gleeson (University of Melbourne, Australia) for the Myc-tagged Golgin-245 construct; Dr. J. Stow (University of Queensland, Brisbane, Australia) or the GFP-tagged E-cadherin construct; Dr. B. Goud (Institut Curie, Paris, France) for the mCherry-tagged Rab11 construct; Dr. M. A. De Matteis (Telethon Institute of Genetics and Medicine, Pozzuoli, Italy) for providing the FLAG-tagged WT Golgin-97 construct; Dr. S. Di Paola (National Research Council, Naples) for discussions and critical reading of the manuscript; Mr. G. Turacchio for performing the microinjection and VSVG transport assays; Dr. G. Catara for initial help in cloning; Dr. N. Dathan for help in protein purification; the BioImaging Facility at the Institute for Endocrinology and Experimental Oncology "G. Salvatore" for support in imaging and data analysis; and the Italian Association for Cancer Research (AIRC) (IG18776 to D.C.; IG20786 to A.L.), AIRC-Fondazione Cariplo TRansforming IDEas in Oncological Research Project (IG17524 to C.V.), "Identificazione di agenti bioattivi da prodotti naturali di origine animale e vegetale (PRONAT), "Progetti di rilevante interesse nazionale" (PRIN) 20177XJCHX Projects, and "Sviluppo di approcci terapeutici innovativi per patologie neoplastiche resistenti ai trattamenti" (SATIN) and Campania Imaging Infrastructure for Research in Oncology (CIRO)-Operative Regional Program (POR) Projects 2014 to 2021 for supporting our work.

1. D. Corda, M. Di Girolamo, Functional aspects of protein mono-ADP-ribosylation. *EMBO J.* **22**, 1953–1958 (2003).
2. W. L. Kraus, PARPs and ADP-ribosylation: 50 years … and counting. *Mol. Cell* **58**, 902–910 (2015).
3. S. Shall, ADP-ribosylation reactions. *Biochimie* **77**, 313–318 (1995).
4. L. Aravind, D. Zhang, R. F. de Souza, S. Anand, L. M. Iyer, The natural history of ADP-ribosyltransferases and the ADP-ribosylation system. *Curr. Top. Microbiol. Immunol.* **384**, 3–32 (2015).
5. J. Abplanalp, M. O. Hottiger, Cell fate regulation by chromatin ADP-ribosylation. *Semin. Cell Dev. Biol.* **63**, 114–122 (2017).
6. M. O. Hottiger, Nuclear ADP-ribosylation and its role in chromatin plasticity, cell differentiation, and epigenetics. *Annu. Rev. Biochem.* **84**, 227–263 (2015).
7. R. Krishnakumar, W. L. Kraus, The PARP side of the nucleus: Molecular actions, physiological outcomes, and clinical targets. *Mol. Cell* **39**, 8–24 (2010).
8. B. Lüscher *et al.*, ADP-ribosyltransferases, an update on function and nomenclature. *FEBS J.*, 10.1111/febs.16142 (2021).
9. H. Otto *et al.*, In silico characterization of the family of PARP-like poly(ADP-ribosyl)-transferases (pARTs). *BMC Genomics* **6**, 139 (2005).
10. D. M. Gill, A. M. Pappenheimer Jr, R. Brown, J. T. Kurnick, Studies on the mode of action of diphtheria toxin. VII. Toxin-stimulated hydrolysis of nicotinamide adenine dinucleotide in mammalian cell extracts. *J. Exp. Med.* **129**, 1–21 (1969).
11. J. Moss, M. Vaughan, Mechanism of action of choleragen. Evidence for ADP-ribosyltransferase activity with arginine as an acceptor. *J. Biol. Chem.* **252**, 2455–2457 (1977).
12. N. Dani *et al.*, Mono-ADP-ribosylation of the G protein betagamma dimer is modulated by hormones and inhibited by Arf6. *J. Biol. Chem.* **286**, 5995–6005 (2011).
13. R. Lupi *et al.*, Endogenous mono-ADP-ribosylation of the free Gbetagamma prevents stimulation of phosphoinositide 3-kinase-gamma and phospholipase C-beta2 and is activated by G-protein-coupled receptors. *Biochem. J.* **367**, 825–832 (2002).
14. R. Lupi, D. Corda, M. Di Girolamo, Endogenous ADP-ribosylation of the G protein beta subunit prevents the inhibition of type 1 adenylyl cyclase. *J. Biol. Chem.* **275**, 9418–9424 (2000).
15. M. Seman *et al.*, NAD-induced T cell death: ADP-ribosylation of cell surface proteins by ART2 activates the cytolytic P2X7 purinoceptor. *Immunity* **19**, 571–582 (2003).
16. I. J. Okazaki, J. Moss, Characterization of glycosylphosphatidylinositiol-anchored, secreted, and intracellular vertebrate mono-ADP-ribosyltransferases. *Annu. Rev. Nutr.* **19**, 485–509 (1999).
17. S. C. Buch-Larsen *et al.*, Mapping physiological ADP-ribosylation using activated ion electron transfer dissociation. *Cell Rep.* **32**, 108176 (2020).
18. M. S. Cohen, P. Chang, Insights into the biogenesis, function, and regulation of ADP-ribosylation. *Nat. Chem. Biol.* **14**, 236–243 (2018).
19. R. Gupte, Z. Liu, W. L. Kraus, PARPs and ADP-ribosylation: Recent advances linking molecular functions to biological outcomes. *Genes Dev.* **31**, 101–126 (2017).
20. X. Luo, W. L. Kraus, On PAR with PARP: Cellular stress signaling through poly(ADP-ribose) and PARP-1. *Genes Dev.* **26**, 417–432 (2012).
21. G. Catara *et al.*, PARP1-produced poly-ADP-ribose causes the PARP12 translocation to stress granules and impairment of Golgi complex functions. *Sci. Rep.* **7**, 14035 (2017).
22. A. K. Leung, Poly(ADP-ribose): An organizer of cellular architecture. *J. Cell Biol.* **205**, 613–619 (2014).
23. A. K. Leung *et al.*, Poly(ADP-ribose) regulates stress responses and microRNA activity in the cytoplasm. *Mol. Cell* **42**, 489–499 (2011).
24. S. Di Paola, M. Micaroni, G. Di Tullio, R. Buccione, M. Di Girolamo, PARP16/ARTD15 is a novel endoplasmic-reticulum-associated mono-ADP-ribosyltransferase that interacts with, and modifies karyopherin-β1. *PLoS One* **7**, e37352 (2012).
25. M. Jwa, P. Chang, PARP16 is a tail-anchored endoplasmic reticulum protein required for the PERK- and IRE1α-mediated unfolded protein response. *Nat. Cell Biol.* **14**, 1223–1230 (2012).

26. G. Grimaldi, D. Corda, ADP-ribosylation and intracellular traffic: An emerging role for PARP enzymes. *Biochem. Soc. Trans.* **47**, 357–370 (2019).
27. N. W. Chi, H. F. Lodish, Tankyrase is a Golgi-associated mitogen-activated protein kinase substrate that interacts with IRAP in GLUT4 vesicles. *J. Biol. Chem.* **275**, 38437–38444 (2000).
28. H. L. Guo *et al.*, The Axin/TNKS complex interacts with KIF3A and is required for insulin-stimulated GLUT4 translocation. *Cell Res.* **22**, 1246–1257 (2012).
29. Z. Su, V. Deshpande, D. E. James, J. Stöckli, Tankyrase modulates insulin sensitivity in skeletal muscle cells by regulating the stability of GLUT4 vesicle proteins. *J. Biol. Chem.* **293**, 8578–8587 (2018).
30. T. Y. Yeh, J. I. Sbodio, Z. Y. Tsun, B. Luo, N. W. Chi, Insulin-stimulated exocytosis of GLUT4 is enhanced by IRAP and its partner tankyrase. *Biochem. J.* **402**, 279–290 (2007).
31. S. Atasheva, M. Akhrymuk, E. I. Frolova, I. Frolov, New PARP gene with an anti-alphavirus function. *J. Virol.* **86**, 8147–8160 (2012).
32. S. Atasheva, E. I. Frolova, I. Frolov, Interferon-stimulated poly(ADP-ribose) polymerases are potent inhibitors of cellular translation and virus replication. *J. Virol.* **88**, 2116–2130 (2014).
33. L. Li *et al.*, *PARP12* suppresses Zika virus infection through PARP-dependent degradation of NS1 and NS3 viral proteins. *Sci. Signal.* **11**, eaas9332 (2018).
34. I. Welsby *et al.*, PARP12, an interferon-stimulated gene involved in the control of protein translation and inflammation. *J. Biol. Chem.* **289**, 26642–26657 (2014).
35. G. Grimaldi *et al.*, PARPs and PAR as novel pharmacological targets for the treatment of stress granule-associated disorders. *Biochem. Pharmacol.* **167**, 64–75 (2019).
36. M. A. De Matteis, A. Luini, Exiting the Golgi complex. *Nat. Rev. Mol. Cell Biol.* **9**, 273–284 (2008).
37. Y. Guo, D. W. Sirkis, R. Schekman, Protein sorting at the *trans*-Golgi network. *Annu. Rev. Cell Dev. Biol.* **30**, 169–206 (2014).
38. J. Z. A. Tan, P. A. Gleeson, Cargo sorting at the *trans*-Golgi network for shunting into specific transport routes: Role of Arf small G proteins and adaptor complexes. *Cells* **8**, E531 (2019).
39. A. Hausser *et al.*, Protein kinase D regulates vesicular transport by phosphorylating and activating phosphatidylinositol-4 kinase IIIbeta at the Golgi complex. *Nat. Cell Biol.* **7**, 880–886 (2005).
40. M. Liljedahl *et al.*, Protein kinase D regulates the fission of cell surface destined transport carriers from the *trans*-Golgi network. *Cell* **104**, 409–420 (2001).
41. P. Coopman, A. Djiane, Adherens junction and E-cadherin complex regulation by epithelial polarity. *Cell. Mol. Life Sci.* **73**, 3535–3553 (2016).
42. U. Tepass, The apical polarity protein network in *Drosophila* epithelial cells: Regulation of polarity, junctions, morphogenesis, cell growth, and survival. *Annu. Rev. Cell Dev. Biol.* **28**, 655–685 (2012).
43. G. Boncompain *et al.*, Synchronization of secretory protein traffic in populations of cells. *Nat. Methods* **9**, 493–498 (2012).
44. E. V. Polishchuk, A. Di Pentima, A. Luini, R. S. Polishchuk, Mechanism of constitutive export from the Golgi: Bulk flow via the formation, protrusion, and en bloc cleavage of large *trans*-Golgi network tubular domains. *Mol. Biol. Cell* **14**, 4470–4485 (2003).
45. C. Valente *et al.*, A 14-3-3γ dimer-based scaffold bridges CtBP1-S/BARS to PI(4)KIIIβ to regulate post-Golgi carrier formation. *Nat. Cell Biol.* **14**, 343–354 (2012).
46. A. Pagliuso *et al.*, Golgi membrane fission requires the CtBP1-S/BARS-induced activation of lysophosphatidic acid acyltransferase δ. *Nat. Commun.* **7**, 12148 (2016).
47. A. Müsch, H. Xu, D. Shields, E. Rodriguez-Boulan, Transport of vesicular stomatitis virus G protein to the cell surface is signal mediated in polarized and nonpolarized cells. *J. Cell Biol.* **133**, 543–558 (1996).
48. C. Yeaman *et al.*, Protein kinase D regulates basolateral membrane protein exit from *trans*-Golgi network. *Nat. Cell Biol.* **6**, 106–112 (2004).
49. T. Yoshimori, P. Keller, M. G. Roth, K. Simons, Different biosynthetic transport routes to the plasma membrane in BHK and CHO cells. *J. Cell Biol.* **133**, 247–256 (1996).
50. J. J. H. Shin, A. K. Gillingham, F. Begum, J. Chadwick, S. Munro, TBC1D23 is a bridging factor for endosomal vesicle capture by Golgins at the *trans*-Golgi. *Nat. Cell Biol.* **19**, 1424–1432 (2017).
51. M. Wong, S. Munro, Membrane trafficking. The specificity of vesicle traffic to the Golgi is encoded in the Golgin coiled-coil proteins. *Science* **346**, 1256898 (2014).
52. J. G. Lock, L. A. Hammond, F. Houghton, P. A. Gleeson, J. L. Stow, E-cadherin transport from the *trans*-Golgi network in tubulovesicular carriers is selectively regulated by Golgin-97. *Traffic* **6**, 1142–1156 (2005).
53. M. Wong, A. K. Gillingham, S. Munro, The Golgin coiled-coil proteins capture different types of transport carriers via distinct N-terminal motifs. *BMC Biol.* **15**, 3 (2017).
54. N. Dani *et al.*, Combining affinity purification by ADP-ribose-binding macro domains with mass spectrometry to define the mammalian ADP-ribosyl proteome. *Proc. Natl. Acad. Sci. U.S.A.* **106**, 4243–4248 (2009).
55. G. Grimaldi, G. Catara, C. Valente, D. Corda, In vitro techniques for ADP-ribosylated substrate identification. *Methods Mol. Biol.* **1813**, 25–40 (2018).
56. M. Lo Monte, C. Manelfi, M. Gemei, D. Corda, A. R. Beccari, ADPredict: ADP-ribosylation site prediction based on physicochemical and structural descriptors. *Bioinformatics* **34**, 2566–2574 (2018).
57. G. V. Beznoussenko *et al.*, Transport of soluble proteins through the Golgi occurs by diffusion via continuities across cisternae. *eLife* **3**, e02009 (2014).
58. J. Trigg, K. Gutwin, A. E. Keating, B. Berger, Multicoil2: Predicting coiled coils and their oligomerization states from sequence in the twilight zone. *PLoS One* **6**, e23519 (2011).
59. J. Jing *et al.*, FIP1/RCP binding to Golgin-97 regulates retrograde transport from recycling endosomes to the *trans*-Golgi network. *Mol. Biol. Cell* **21**, 3041–3053 (2010).
60. A. J. Lindsay, M. W. McCaffrey, The C2 domains of the class I Rab11 family of interacting proteins target recycling vesicles to the plasma membrane. *J. Cell Sci.* **117**, 4365–4375 (2004).
61. C. L. Baron, V. Malhotra, Role of diacylglycerol in PKD recruitment to the TGN and protein transport to the plasma membrane. *Science* **295**, 325–328 (2002).
62. A. K. Gillingham, S. Munro, Finding the Golgi: Golgin coiled-coil proteins show the way. *Trends Cell Biol.* **26**, 399–408 (2016).
63. T. M. Witkos, M. Lowe, The Golgin family of coiled-coil tethering proteins. *Front. Cell Dev. Biol.* **3**, 86 (2016).
64. L. Kjer-Nielsen, R. D. Teasdale, C. van Vliet, P. A. Gleeson, A novel Golgi-localisation domain shared by a class of coiled-coil peripheral membrane proteins. *Curr. Biol.* **9**, 385–388 (1999).
65. S. Munro, B. J. Nichols, The GRIP domain—A novel Golgi-targeting domain found in several coiled-coil proteins. *Curr. Biol.* **9**, 377–380 (1999).
66. M. C. Derby *et al.*, Mammalian GRIP domain proteins differ in their membrane binding properties and are recruited to distinct domains of the TGN. *J. Cell Sci.* **117**, 5865–5874 (2004).
67. L. Lu, W. Hong, Interaction of Arl1-GTP with GRIP domains recruits autoantigens Golgin-97 and Golgin-245/p230 onto the Golgi. *Mol. Biol. Cell* **14**, 3767–3781 (2003).
68. A. S. Burguete, T. D. Fenn, A. T. Brunger, S. R. Pfeffer, Rab and Arl GTPase family members cooperate in the localization of the Golgin GCC185. *Cell* **132**, 286–298 (2008).
69. F. J. Houghton, P. L. Chew, S. Lodeho, B. Goud, P. A. Gleeson, The localization of the Golgin GCC185 is independent of Rab6A/A′ and Arl1. *Cell* **138**, 787–794 (2009).
70. P. Y. Cheung, S. R. Pfeffer, Transport vesicle tethering at the *trans* Golgi network: Coiled coil proteins in action. *Front. Cell Dev. Biol.* **4**, 18 (2016).
71. Z. Z. Lieu *et al.*, A *trans*-Golgi network Golgin is required for the regulated secretion of TNF in activated macrophages in vivo. *Proc. Natl. Acad. Sci. U.S.A.* **105**, 3351–3356 (2008).
72. T. K. Taneja, D. Ma, B. Y. Kim, P. A. Welling, Golgin-97 targets ectopically expressed inward rectifying potassium channel, Kir2.1, to the *trans*-Golgi network in COS-7 cells. *Front. Physiol.* **9**, 1070 (2018).
73. F. A. Barr, B. Short, Golgins in the structure and dynamics of the Golgi apparatus. *Curr. Opin. Cell Biol.* **15**, 405–413 (2003).
74. N. Muschalik, S. Munro, Golgins. *Curr. Biol.* **28**, R374–R376 (2018).
75. J. G. Lock, J. L. Stow, Rab11 in recycling endosomes regulates the sorting and basolateral transport of E-cadherin. *Mol. Biol. Cell* **16**, 1744–1755 (2005).
76. R. Di Martino, L. Sticco, A. Luini, Regulation of cargo export and sorting at the *trans*-Golgi network. *FEBS Lett.* **593**, 2306–2318 (2019).
77. C. Kienzle, J. von Blume, Secretory cargo sorting at the *trans*-Golgi network. *Trends Cell Biol.* **24**, 584–593 (2014).
78. M. Pakdel, J. von Blume, Exploring new routes for secretory protein export from the *trans*-Golgi network. *Mol. Biol. Cell* **29**, 235–240 (2018).
79. A. H. Crevenna *et al.*, Secretory cargo sorting by Ca^{2+}-dependent Cab45 oligomerization at the *trans*-Golgi network. *J. Cell Biol.* **213**, 305–314 (2016).
80. Y. Wakana *et al.*, A new class of carriers that transport selective cargo from the *trans* Golgi network to the cell surface. *EMBO J.* **31**, 3976–3990 (2012).
81. L. Chen, B. Liu, Relationships between stress granules, oxidative stress, and neurodegenerative diseases. *Oxid. Med. Cell. Longev.* **2017**, 1809592 (2017).
82. E. Prieto-García, C. V. Díaz-García, I. García-Ruiz, M. T. Agulló-Ortuño, Epithelial-to-mesenchymal transition in tumor progression. *Med. Oncol.* **34**, 122 (2017).
83. L. Brüser, S. Bogdan, Adherens junctions on the move—Membrane trafficking of E-cadherin. *Cold Spring Harb. Perspect. Biol.* **9**, a029140 (2017).
84. F. Palacios, J. S. Tushir, Y. Fujita, C. D'Souza-Schorey, Lysosomal targeting of E-cadherin: A unique mechanism for the down-regulation of cell-cell adhesion during epithelial to mesenchymal transitions. *Mol. Cell. Biol.* **25**, 389–402 (2005).